TU Delft

Delft University of Technology

Microscopy-based single-cell proteomic profiling reveals heterogeneity in DNA damage response dynamics

Su, Pin Rui; You, Li; Beerens, Cecile; Bezstarosti, Karel; Demmers, Jeroen; Pabst, Martin; Kanaar, Roland; Hsu, Cheng Chih; Chien, Miao Ping

DOI
10.1016/j.crmeth.2022.100237

Publication date
2022

Document Version
Final published version

Published in
Cell Reports Methods

Citation (APA)
Su, P. R., You, L., Beerens, C., Bezstarosti, K., Demmers, J., Pabst, M., Kanaar, R., Hsu, C. C., & Chien, M. P. (2022). Microscopy-based single-cell proteomic profiling reveals heterogeneity in DNA damage response dynamics. *Cell Reports Methods*, *2*(6), Article 100237. https://doi.org/10.1016/j.crmeth.2022.100237

Important note
To cite this publication, please use the final published version (if applicable).
Please check the document version above.

Copyright
Other than for strictly personal use, it is not permitted to download, forward or distribute the text or part of it, without the consent of the author(s) and/or copyright holder(s), unless the work is under an open content license such as Creative Commons.

Takedown policy
Please contact us and provide details if you believe this document breaches copyrights.
We will remove access to the work immediately and investigate your claim.

This work is downloaded from Delft University of Technology.
For technical reasons the number of authors shown on this cover page is limited to a maximum of 10.

Cell Reports
Methods

Report

Microscopy-based single-cell proteomic profiling reveals heterogeneity in DNA damage response dynamics

Graphical abstract

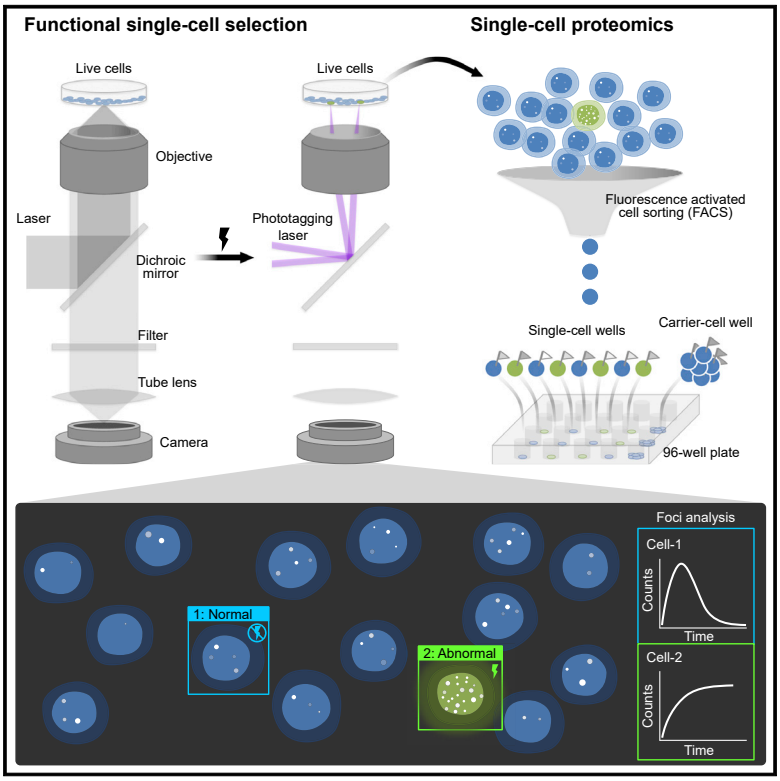

Highlights

- Functional single-cell proteomics links proteomes with phenotypes of interest
- Real-time cell tracking and intracellular dynamics analysis identify abnormal DDR
- PDS5A contributes to abnormal DDR and helps cells survive after ionizing radiation

Authors

Pin-Rui Su, Li You, Cecile Beerens, ..., Roland Kanaar, Cheng-Chih Hsu, Miao-Ping Chien

Correspondence

m.p.chien@erasmusmc.nl

In brief

Su et al. develop a microscopy-based single-cell proteomic-profiling method to link single-cell proteomes with phenotypes of interest. The method combines a custom-built microscope, real-time image analysis, single-cell selection (phototagging) and isolation, and single-cell proteomics. The authors applied it to identify the key protein driving abnormal, radiation-induced DNA damage response.

Su et al., 2022, Cell Reports Methods 2, 100237
June 20, 2022 © 2022 The Author(s).
https://doi.org/10.1016/j.crmeth.2022.100237

CellPress

Cell Reports Methods

CellPress
OPEN ACCESS

Report

Microscopy-based single-cell proteomic profiling reveals heterogeneity in DNA damage response dynamics

Pin-Rui Su,[1,2,5] Li You,[1,2] Cecile Beerens,[1,2] Karel Bezstarosti,[3] Jeroen Demmers,[3] Martin Pabst,[4] Roland Kanaar,[1,2,6] Cheng-Chih Hsu,[5,7] and Miao-Ping Chien[1,2,6,7,8,*]

[1]Department of Molecular Genetics, Erasmus University Medical Center, Rotterdam, the Netherlands
[2]Erasmus MC Cancer Institute, Rotterdam, the Netherlands
[3]Proteomics Core Facility, Erasmus University Medical Center, Rotterdam, the Netherlands
[4]Department of Biotechnology, Delft University of Technology, Delft, the Netherlands
[5]Department of Chemistry, National Taiwan University, Taipei, Taiwan
[6]Oncode Institute, Utrecht, the Netherlands
[7]Senior author
[8]Lead contact
*Correspondence: m.p.chien@erasmusmc.nl
https://doi.org/10.1016/j.crmeth.2022.100237

MOTIVATION Tumor heterogeneity is an important source of cancer-therapy resistance. Single-cell proteomics has the potential to decipher protein content leading to heterogeneous cellular phenotypes. Mass-spectrometry-based single-cell proteomics methods like SCoPE-MS are recently developed, promising, unbiased proteomic-profiling techniques and allow profiling single cells with >1,000 proteins/cell in a high-throughput manner. However, these methods lack the capability to link single-cell proteomes with phenotypes of interest. Here, we developed a microscopy-based functional single-cell proteomic-profiling technology to bridge this gap and applied it to discover the key protein that contributes to radiation-induced, abnormal DNA damage response.

SUMMARY

Single-cell proteomics has the potential to decipher tumor heterogeneity, and a method like single-cell proteomics by mass spectrometry (SCoPE-MS) allows profiling several tens of single cells for >1,000 proteins per cell. This method, however, cannot link the proteome of individual cells with phenotypes of interest. Here, we developed a microscopy-based functional single-cell proteomic-profiling technology, called FUNpro, to address this. FUNpro enables screening, identification, and isolation of single cells of interest in a real-time fashion, even if the phenotypes are dynamic or the cells of interest are rare. We applied FUNpro to proteomically profile a newly identified small subpopulation of U2OS osteosarcoma cells displaying an abnormal, prolonged DNA damage response (DDR) after ionizing radiation (IR). With this, we identified the PDS5A protein contributing to the abnormal DDR dynamics and helping the cells survive after IR.

INTRODUCTION

A high degree of cellular heterogeneity underlies biological processes like tumorigenesis or differentiation. In the past several years, single-cell profiling technologies have revolutionized biological and biomedical research into rare cells or subpopulations of cells (Kolodziejczyk et al., 2015; Grün et al., 2015). Single-cell RNA or DNA sequencing technology has developed much more rapidly than single-cell proteomics (Vistain and Tay, 2021). However, to gain mechanistic understanding of cellular processes like the DNA damage response (DDR), measuring and quantifying the effector/active molecules, namely the proteins, is imperative (Vistain and Tay, 2021). Single-cell proteomics by mass spectrometry (SCoPE-MS) is a recently developed, antibody-independent single-cell proteomics technique (Budnik et al., 2018); this approach has gradually become popular because it is an unbiased proteomic-profiling method (antibody independent) and enables identification of >1,000 proteins in single cells. Cell sorting is often applied before SCoPE-MS, and cell selection based on static features has advanced rapidly in recent years (Nitta et al., 2018). However, a method to link measured proteomes of single cells to more interesting cellular,

This is an open access article under the CC BY-NC-ND license (http://creativecommons.org/licenses/by-nc-nd/4.0/).

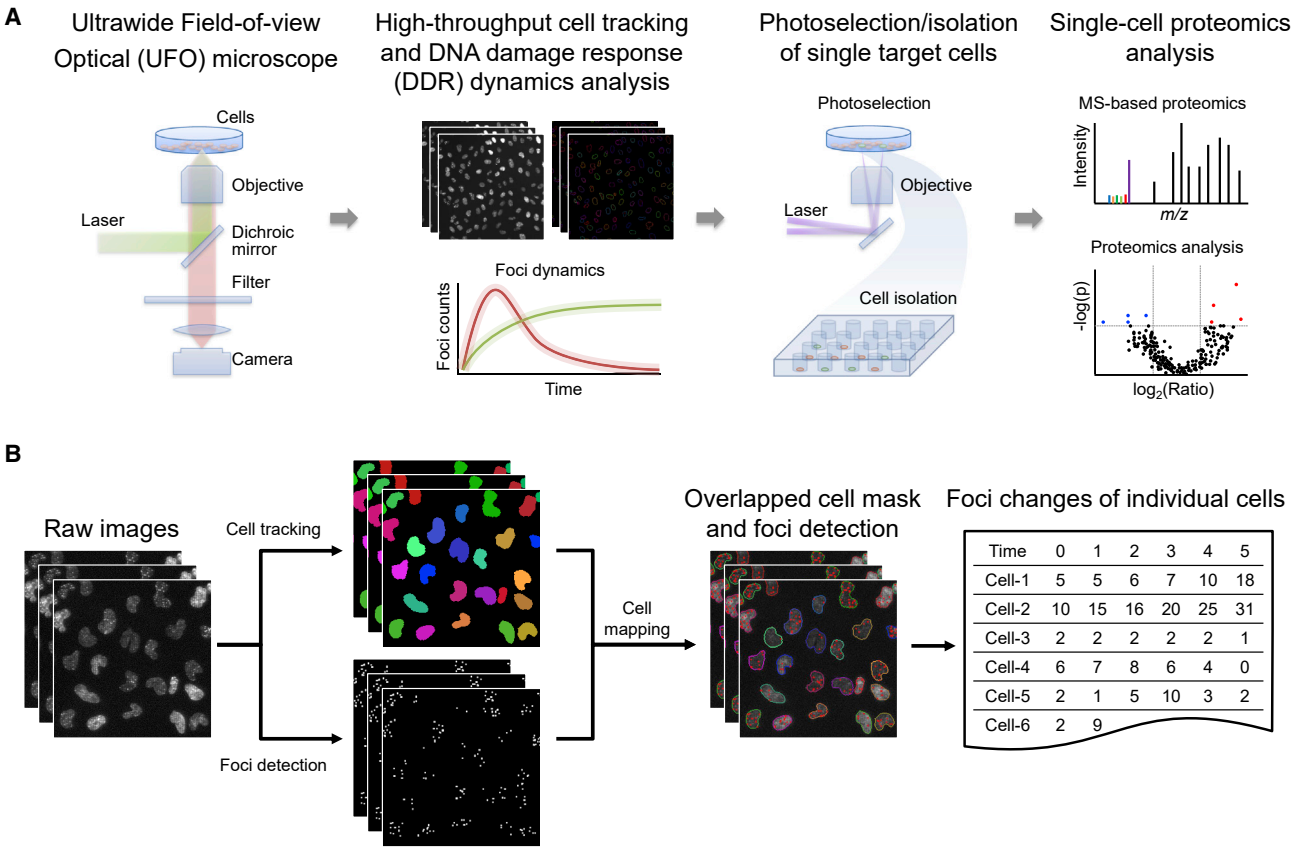

Time	0	1	2	3	4	5
Cell-1	5	5	6	7	10	18
Cell-2	10	15	16	20	25	31
Cell-3	2	2	2	2	2	1
Cell-4	6	7	8	6	4	0
Cell-5	2	1	5	10	3	2
Cell-6	2	9				

Figure 1. Outline of the developed functional single-cell proteomic profiling (FUNpro) pipeline

(A) FUNpro pipeline: cells were high-throughput screened under the UFO microscope followed by real-time cell tracking and intracellular dynamics analysis to identify cells of interest; desired cells were then selectively photolabeled followed by cell sorting before being subjected to single-cell proteomic measurements and analysis.

(B) Schematic of high-throughput identification and selection of target cells via an automated image processing and analysis algorithm.

intracellular, and intercellular dynamics (for example, migration, longitudinal protein dynamics, multicell interaction), static features, and combinations of both does not yet exist and would significantly expand on the applications for single-cell proteomics, allowing the investigation of novel mechanistic questions.

RESULTS

FUNpro links single-cell proteomes with phenotypes of interest like abnormal DDR

Here, we introduce a technology, called functional single-cell proteomic profiling (FUNpro; Figure 1), that (1) enables screening a population containing a large quantity of cancer cells (>10^3) with high spatiotemporal resolution via a custom-built ultrawide field-of-view optical (UFO) microscope, (2) allows real-time identifying cells with different (intra)cellular dynamics via an integrated automatic cell-tracking algorithm (Figure 1B), and (3) permits separating different phenotypes of cells with selective photolabeling of desired cells followed by cell sorting and single-cell proteomic profiling. With FUNpro, we can stratify or pre-select cells ahead of time based on any microscopically observable cellular and/or intracellular behaviors before subjecting them to single-cell proteomic measurements.

An example of a heterogeneous phenomenon that can be investigated using this technique is DDR. DDR, triggered by DNA breaks or DNA double-strand breaks (DSBs), leads to a series of DDR proteins to assemble and act on damaged DNA sites to maintain genomic integrity (Iwabuchi et al., 2003; Panier and Boulton, 2014; Rothkamm et al., 2015). One of the key DDR proteins, tumor suppressor p53-binding protein 1 (53BP1), accumulates and forms oligomers (53BP1 foci) on DSBs to regulate DNA repair and has been used as a DDR indicator in response to DSBs (Iwabuchi et al., 2003; Panier and Boulton, 2014; Rothkamm et al., 2015). Unrepaired or misrepaired DSBs often lead to mutations or chromosomal rearrangements that can result in cell death or oncogenic transformation that can promote tumor progression and evolution (Hakem, 2008). In addition, efficient DDR, caused by, among others, overactive or overexpressed DDR proteins, can lead to cancer cell survival in response to treatment (Hakem, 2008). These various scenarios regarding DDR or repair mechanisms can contribute to tumor heterogeneity and lead to different cell fates (cell death or tumor

CellPress
OPEN ACCESS

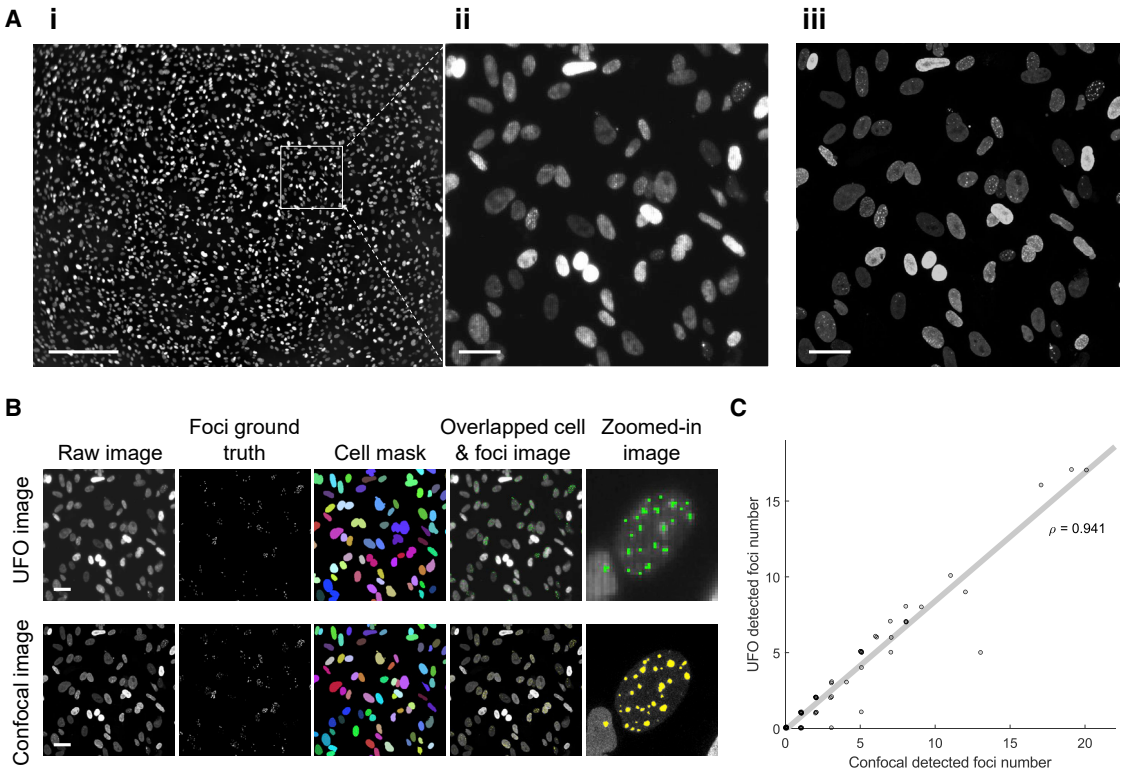

Figure 2. DDR foci detected by the UFO or confocal microscope

(A) (i–iii) UFO image of U2OS-53BP1-mScarlet cells. (i) A full field-of-view image. Scale bar: 500 μm. (ii) A zoomed-in image from (i). Scale bar: 50 μm. (iii) A confocal microscopic image (same field-of-view as in ii). Scale bar: 50 μm.

(B) The same field-of-view of the same dish was imaged under the UFO or confocal microscope. The foci ground truth was manually annotated. Scale bar: 50 μm.

(C) Spearman correlation analysis of the foci number per cell between the UFO image and the confocal image (foci diameter larger than 1 μm with a SNR larger than 2.0). Spearman correlation coefficient (ρ) was indicated.

progression); hence, it is crucial to decipher causative underlying mechanisms of heterogeneous dynamics of DDR.

As a proof of concept, we applied FUNpro to profile and investigate a subpopulation of U2OS cells displaying abnormal DDR induced by ionizing radiation (IR). We used U2OS cells expressing 53BP1-mScarlet as a model system and monitored IR-induced DDR dynamics via 53BP1 foci changes, imaged through clustered mScarlet-fluorescence. To screen a large quantity of cells and identify subpopulations of cells with different intracellular 53BP1 foci changes over time, we implemented the UFO microscope (You et al., 2022) in the FUNpro pipeline (Figure 1A) to image thousands of cells with 0.8 μm spatial resolution, sufficient to resolve nuclear DDR foci. Given that DDR foci has so far mainly been detected using confocal microscopy, we confirmed that the foci detected by UFO show a high correlation (Spearman's correlation ρ = 0.94; Figure 2C) with the foci detected by confocal microscopy (with a size larger than 1 μm in diameter and a signal-to-noise ratio [SNR] higher than 2.0) (Figure 2). We then developed and implemented an automatic DDR foci-tracking algorithm (STAR methods; Figures 1B and S1; Table S1) in the modified tracking with Gaussian mixture model (mTGMM [You et al., 2022]) cell-tracking algorithm to quantify changes in DDR foci while tracking cellular movement in a real-time fashion. We tracked individual cell migration and division and intracellular dynamics for thousands of cells (~57,000 cells/min) to register foci dynamics for individual cells over hundreds of image frames (24 h of imaging; Figure 1B). We applied a phototagging technique (STAR methods) to selectively photolabel cells of interest for cell sorting with fluorescence-activated cell sorting (FACS). Finally, SCoPE-MS was applied to quantify the proteins of single cells, and a differential protein analysis was computed by comparing the proteins from the cells of interest with the control cells.

After irradiating U2OS-53BP1-mScarlet cells with 2 Gy IR, cells were immediately subjected to UFO for data acquisition and imaging for 24 h (3 min/frame). We then applied the integrated cell and DDR foci-tracking algorithm (STAR methods; Figures 1B and S1; Table S1) to analyze the 24 h time-lapse movie of U2OS-53BP1-mScarlet cells (Figure 3). After analyzing ~10^3 irradiated cells, we identified two different groups of cells based on the dynamics of DDR foci formation (53BP1-mScarlet foci) (Figures 3C and 3D). One group (group 1) had a peak amount of DDR foci at 4–6 h after irradiation, immediately followed by decay in foci number at 6 h (we call this an up-and-down foci trend or normal DDR dynamics, based on published observations [Georgescu et al., 2015; Kilic et al., 2019; Sollazzo et al., 2018]). The other group (group 2) had rising DDR foci counts at 4–6 h without decaying until at least 24 h (we call this

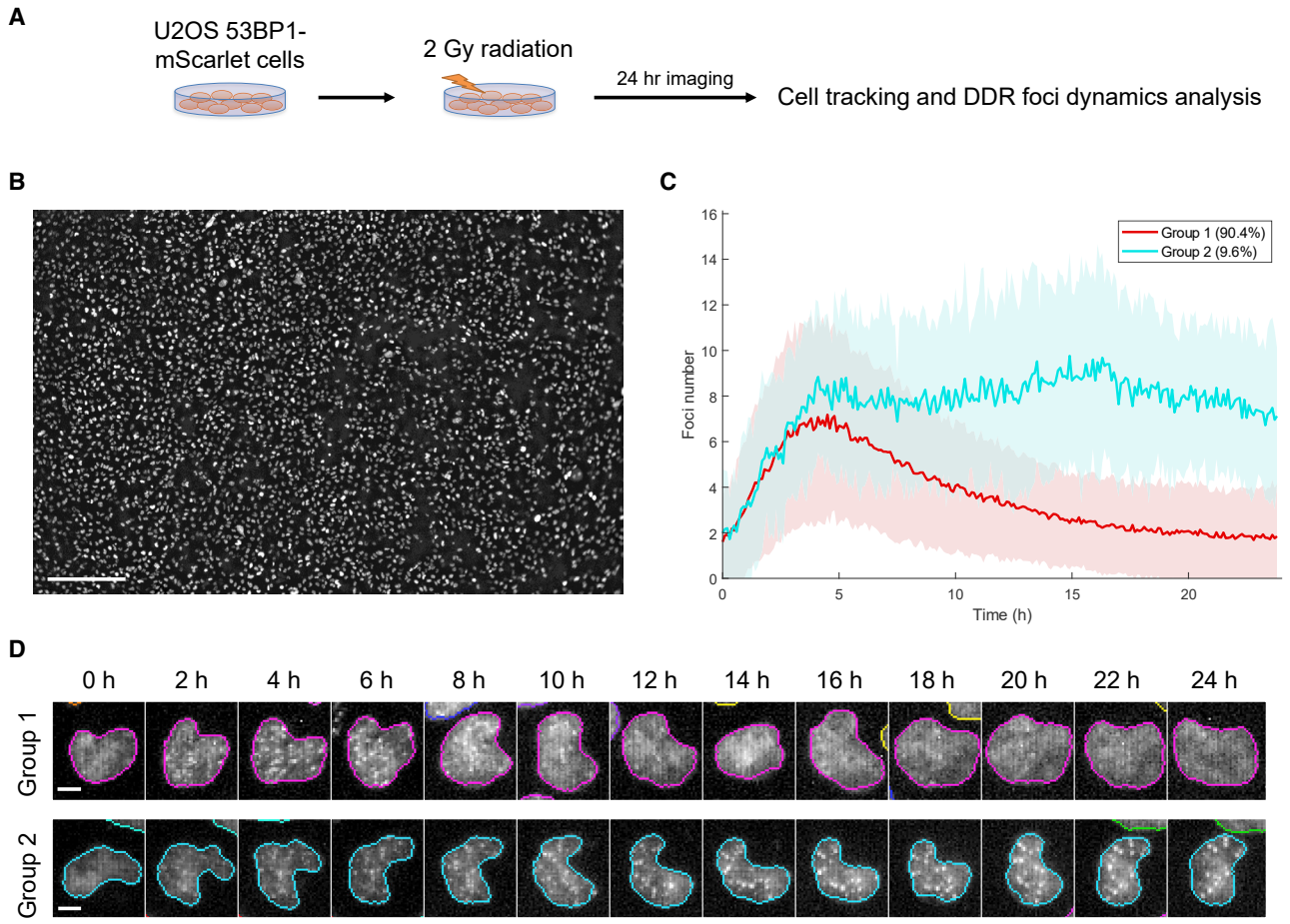

Figure 3. 53BP1 foci dynamics tracking (U2OS-53BP1-mScarlet cells) for 24 h after 2 Gy irradiation under the UFO microscope

(A) Schematic workflow of live-cell imaging on the UFO microscope.

(B) A representative UFO microscopic image of irradiated U2OS-53BP1-mScarlet cells. Scale bar: 500 μm. N = ~3,000 cells.

(C) 53BP1 foci dynamics of two groups of cells over the course of a day. Solid lines represent the average foci number trend from all the cells of each group. The background, light-color areas represent the standard deviations of the trends.

(D) The zoomed-in images showed the foci changes of representative group 1 and group 2 cells after 1 day of IR. Scale bar: 10 μm.

a rising foci trend or abnormal DDR dynamics) (Figure 3C). The IR-induced DDR dynamics shown in group 1 is the main phenotype reported previously (Georgescu et al., 2015; Kilic et al., 2019; Sollazzo et al., 2018), whereas group 2 has not been reported before, a phenotype that was only revealed after the cluster analysis from analyzing a large quantity of cells (Figure 3). For the cells showing DDR foci changes, 90.4% of the cells belonged to group 1 (up-and-down foci trend; Figure 3C) and 9.6% to group 2 (rising foci trend; Figure 3C). In addition, these two distinct DDR foci dynamic phenotypes were not observed in the absence of IR (data not shown), indicating that the phenotypes were associated with IR-induced DDR.

PDS5A was upregulated in the cells with abnormal IR-induced DDR

To further investigate the group 2 cells, which displayed abnormal, prolonged IR-induced DDR response, we photo-tagged and separated group 2 cells and control group 1 cells (Figure 4A) and performed SCoPE-MS (Budnik et al., 2018) (Figure 4B; the quality and quantitative accuracy of the data are shown in Figures S2 and S3 and STAR methods). We conducted three independent experiments and collected 40 group 1 (up-and-down foci trend) and 40 group 2 (rising foci trend) cells in total after FACS. No clear clusters were found using unsupervised clustering analysis (Figure S4A) because of similar expression profiles between these two groups of cells. With FUNpro's annotation, differential expression analysis could be performed between group 1 and group 2 cells (Figure 4C). After the analysis, two differential proteins (PDS5A and UQCR10) upregulated in group 2 cells (rising DDR foci) were identified and passed the permutation-based false discovery rate (FDR) test (FDR $\leq$ 0.05). In addition, we implemented a cell-cycle scoring analysis from Tirosh et al. (2016) and found that both groups of cells had a similar amount of cells at G1, S, and G2/M phases (STAR methods; Figure S4B and S4C), indicating that these two phenotypes were not caused by cell-cycle effects. Of the two differentially expressed proteins (Figure 4C), only PDS5A (sister chromatid cohesion protein PDS5 homolog A) has been

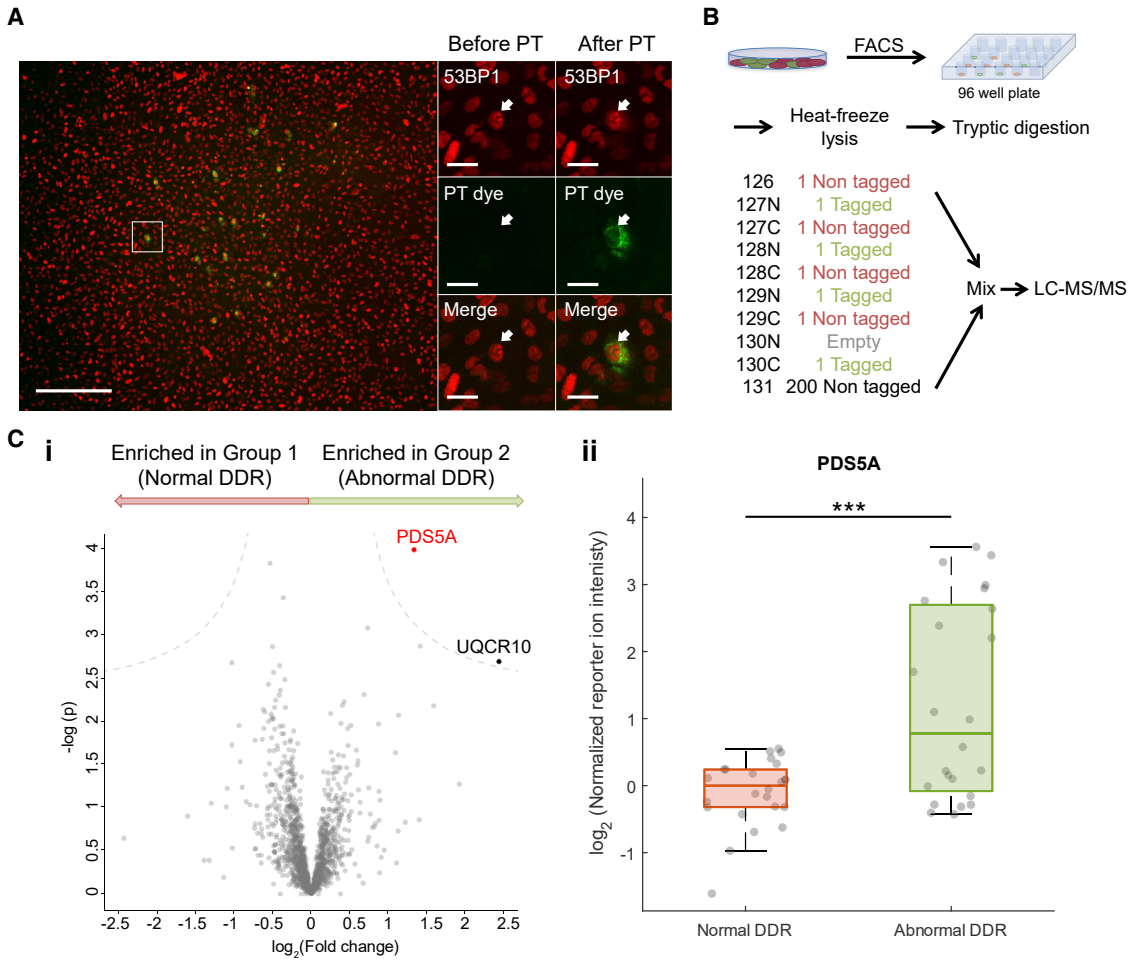

Figure 4. Single-cell quantitative proteomics on group 1 and group 2 cells collected by the FUNpro pipeline

(A) Phototagging of the group 2 cells. Scale bar: 500 μm. The zoomed-in images showed a representative cell (arrow) before and after phototagging. Scale bar: 50 μm. Red, 53BP1; green, phototagging (PT) dye.

(B) Schematic protocol of single-cell proteomics analysis. Four non-tagged cells, four tagged cells, and 200 non-tagged cells (serving as carrier cells) were labeled with respective 10-plex TMT labels as indicated and then mixed into one sample before being subjected to liquid chromatography tandem mass spectrometry (LC-MS/MS). Ten samples, in total 40 group 1 and 40 group 2 cells, were analyzed.

(C) (i) A volcano plot showing proteins enriched either in group 1 (normal DDR) or group 2 (abnormal DDR) cells. Together, 80 cells were pooled into the analysis. Dashed lines show the cutoff value of FDR at 0.05. (ii) DDR-related protein, PDS5A, was found upregulated in group 2 cells.

shown to be related to DDR, as its loss leads to DNA damage (Al-Jomah et al., 2020; Morales et al., 2020). Furthermore, PDS5A is a crucial player in protecting DNA replication forks and therefore maintains genome stability from DNA breaks (Al-Jomah et al., 2020; Morales et al., 2020). We further validated the discovery with immunofluorescence staining (Figure 5), where significantly higher protein expression of PDS5A was found in group 2 cells. In addition, more γH2AX foci (a direct indicator of double-stranded DNA breaks) were also found in group 2 cells (Figure S5A). With these observations, we suspected that group 2 cells displaying the rising DDR foci trend after radiation bore more severe DNA damage (more γH2AX foci; Figure S5A) than group 1 cells and were in the process of rescuing themselves from apoptosis and still survived after 2 days of IR (Figure S5B).

DISCUSSION

In conclusion, we demonstrated a method to screen a large quantity of individual cells, monitor their cellular and intracellular dynamics, and real-time identify cells of interest displaying desired (intra)cellular dynamics followed by single-cell quantitative proteomics. With this, we identified a new subpopulation of U2OS cells displaying abnormal DDR dynamics after IR (rising DDR foci trend) compared with the majority of the cell population (up-and-down foci trend). We also identified the PDS5A protein as contributing to this cellular phenotype and cell survival after IR. With FUNpro, we can pre-select individual cells based on any microscopically observable features or characteristics, enrich the quantity of the desired cells, and link phenotypes of interest to their proteome. Furthermore, FUNpro could potentially

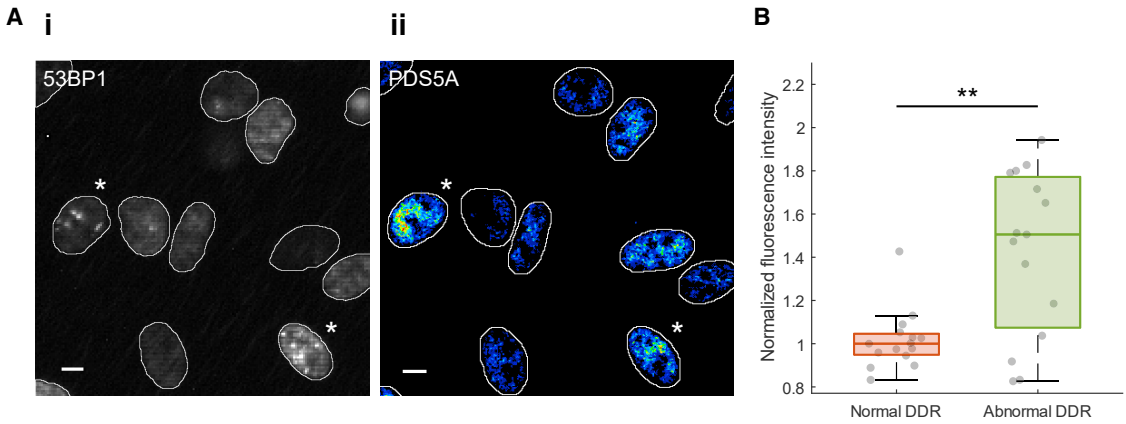

Figure 5. Immunofluorescence validation of the PDS5A protein on group 1 and group 2 (with asterisk) cells

(A) (i) A UFO image of U2OS cells expressing 53BP1-mScarlet (gray). The image was taken after 24 h of IR. Scale bar: 10 μm. (ii) A confocal image of immunofluorescence against the PDS5A protein (16 colored) from the same fieldof-view. Scale bar: 10 μm.

(B) Immunofluorescence quantification of the PDS5A protein on group 1 and group 2 cells. In total, 16 pairs of cells were analyzed with p value lower than 0.01 (Student's t test).

be applied to profile differential proteomes of pooled cells (i.e., 10–20 cells) with phenotypes of interest to increase protein coverage when a sufficient quantity of cells is accessible. The technology has the potential to investigate causative molecular mechanisms of cells displaying different phenotypes even if the cells are rare or dynamic.

Limitations of the study

FUNpro is a microscopy-based single-cell proteomic-profiling method and has the potential to link any phenotypes that are observable under a microscope to the proteomes. However, it relies on the visibility, quantifiability, and relevance of the phenotypes underlying the assays. The method consists of live-cell imaging, real-time image analysis, single-cell selection, single-cell isolation, and single-cell proteomics, and therefore extreme care in each step is needed to have a successful outcome. The technique also relies on sufficient computation power to process images and identify phenotypes of interest in real time. The frame rate of the camera used in the system is 30 frames/second. Should the cellular dynamics be faster than this, they would not be resolvable; visualizing them would require a higher-frame-rate system. FUNpro leverages current state-of-the art single-cell proteomics techniques; therefore, any concerns related to those should be carefully assessed including, among others, the number of carrier cells, automatic gain control, and maximum injection time.

STAR★METHODS

Detailed methods are provided in the online version of this paper and include the following:

- KEY RESOURCES TABLE
- RESOURCE AVAILABILITY
  - Lead contact
  - Materials availability
  - Data and code availability
- EXPERIMENTAL MODEL AND SUBJECT DETAILS
  - U2OS cells
- METHOD DETAILS
  - Ultrawide field-of-view optical microscope
  - Cell preparation, radiation and live imaging on the UFO microscope
  - Target cell photolabeling and isolation
  - Single-cell proteomics
  - Immunofluorescence staining and analysis
- QUANTIFICATION AND STATISTICAL ANALYSIS
  - Automatic foci detection analysis
  - Automatic cell tracking analysis
  - Proteomics analysis
  - Quality and quantitative accuracy of the single-cell proteomics data
  - Statistical analysis

SUPPLEMENTAL INFORMATION

Supplemental information can be found online at https://doi.org/10.1016/j.crmeth.2022.100237.

ACKNOWLEDGMENTS

M.-P.C. acknowledges support from the Oncode Institute, Cancer GenomiCs.nl (CGC), NWO (the Netherlands Organization for Scientific Research) Veni Grant, and Stichting Ammodo and Erasmus MC grant. M.-P.C. appreciates Josephine Nefkens Stichting's support on the UFO microscope. C.-C.H. acknowledges support from the Ministry of Science and Technology (MOST) in Taiwan (Dragon Gate program: 107-2911-I-002-577 and Columbus Program: 108-2636-M-002-008- and 109-2636-M-002-005-). We thank Hanny Odijk for the kind gift of the PB-mScarlet-53BP1 plasmid. We thank Tsung Wai Kan for the assistance on FACS. We thank Daan Brinks for the discussion on the manuscript.

AUTHOR CONTRIBUTIONS

P.-R.S. conducted the experiments, improved the setup, scripted the algorithm for DDR foci dynamics analysis, and analyzed the image analysis data. L.Y. scripted the mTGMM cell tracking algorithm. C.B. contributed to part of

the cell culture preparation for the experiments and the immunofluorescence experiment. K.B. and M.P. performed the mass-spectrometry experiments. R.K. advised on part of the experimental design and data interpretation. P.-R.S., J.D., M.P., C.-C.H., and M.-P.C. advised on and analyzed the single-cell proteomics data. M.-P.C. and P.-R.S. designed most of the experiments. M.-P.C., P.-R.S., and C.-C.H. wrote the paper with input from all authors. M.-P.C. initiated the project. M.-P.C. and C.-C.H. contributed to and supervised all aspects of the project.

DECLARATION OF INTERESTS

The authors declare no competing interests.

Received: August 27, 2021
Revised: April 3, 2022
Accepted: May 23, 2022
Published: June 13, 2022

REFERENCES

Al-Jomah, N., Mukololo, L., Anjum, A., Al Madadha, M., and Patel, R. (2020). Pds5A and Pds5B display non-redundant functions in mitosis and their loss triggers Chk1 activation. Front. Cell Dev. Biol. *8*, 531. https://doi.org/10.3389/fcell.2020.00531.

Budnik, B., Levy, E., Harmange, G., and Slavov, N. (2018). SCoPE-MS: mass spectrometry of single mammalian cells quantifies proteome heterogeneity during cell differentiation. Genome Biol. *19*, 161. https://doi.org/10.1186/s13059-018-1547-5.

Cong, Y., Liang, Y., Motamedchaboki, K., Huguet, R., Truong, T., Zhao, R., Shen, Y., Lopez-Ferrer, D., Zhu, Y., and Kelly, R.T. (2020). Improved single-cell proteome coverage using narrow-bore packed NanoLC columns and ultrasensitive mass spectrometry. Anal. Chem. *92*, 2665–2671. https://doi.org/10.1021/acs.analchem.9b04631.

Cox, J., and Mann, M. (2008). MaxQuant enables high peptide identification rates, individualized p.p.b.-range mass accuracies and proteome-wide protein quantification. Nat. Biotechnol. *26*, 1367–1372. https://doi.org/10.1038/nbt.1511.

Georgescu, W., Osseiran, A., Rojec, M., Liu, Y., Bombrun, M., Tang, J., and Costes, S.V. (2015). Characterizing the DNA damage response by cell tracking algorithms and cell features classification using high-content time-lapse analysis. PLoS One *10*, e0129438. https://doi.org/10.1371/journal.pone.0129438.

Grün, D., Lyubimova, A., Kester, L., Wiebrands, K., Basak, O., Sasaki, N., Clevers, H., and van Oudenaarden, A. (2015). Single-cell messenger RNA sequencing reveals rare intestinal cell types. Nature *525*, 251–255. https://doi.org/10.1038/nature14966.

Hakem, R. (2008). DNA-damage repair; the good, the bad, and the ugly. EMBO J. *27*, 589–605. https://doi.org/10.1038/emboj.2008.15.

Iwabuchi, K., Basu, B.P., Kysela, B., Kurihara, T., Shibata, M., Guan, D., Cao, Y., Hamada, T., Imamura, K., Jeggo, P.A., et al. (2003). Potential role for 53BP1 in DNA end-joining repair through direct interaction with DNA. J. Biol. Chem. *278*, 36487–36495. https://doi.org/10.1074/jbc.m304066200.

Kilic, S., Lezaja, A., Gatti, M., Bianco, E., Michelena, J., Imhof, R., and Altmeyer, M. (2019). Phase separation of 53BP1 determines liquid-like behavior of DNA repair compartments. EMBO J. *38*, e101379. https://doi.org/10.15252/embj.2018101379.

Kolodziejczyk, A.A., Kim, J.K., Svensson, V., Marioni, J.C., and Teichmann, S.A. (2015). The technology and biology of single-cell RNA sequencing. Mol. Cell *58*, 610–620. https://doi.org/10.1016/j.molcel.2015.04.005.

Morales, C., Ruiz-Torres, M., Rodríguez-Acebes, S., Lafarga, V., Rodríguez-Corsino, M., Megías, D., Cisneros, D.A., Peters, J.-M., Méndez, J., and Losada, A. (2020). PDS5 proteins are required for proper cohesin dynamics and participate in replication fork protection. J. Biol. Chem. *295*, 146–157. https://doi.org/10.1074/jbc.ra119.011099.

Nitta, N., Sugimura, T., Isozaki, A., Mikami, H., Hiraki, K., Sakuma, S., Iino, T., Arai, F., Endo, T., Fujiwaki, Y., et al. (2018). Intelligent image-activated cell sorting. Cell *175*, 266–276. https://doi.org/10.1016/j.cell.2018.08.028.

Panier, S., and Boulton, S.J. (2014). Double-strand break repair: 53BP1 comes into focus. Nat. Rev. Mol. Cell Biol. *15*, 7–18. https://doi.org/10.1038/nrm3719.

Rothkamm, K., Barnard, S., Moquet, J., Ellender, M., Rana, Z., and Burdak-Rothkamm, S. (2015). DNA damage foci: meaning and significance. Environ. Mol. Mutagen. *56*, 491–504. https://doi.org/10.1002/em.21944.

Ruusuvuori, P., Aijo, T., Chowdhury, S., Garmendia-Torres, C., Selinummi, J., Birbaumer, M., Dudley, A.M., Pelkmans, L., and Yli-Harja, O. (2010). Evaluation of methods for detection of fluorescence labeled subcellular objects in microscope images. BMC Bioinformatics *11*, 248. https://doi.org/10.1186/1471-2105-11-248.

Schneider, C., Rasband, W., and Eliceiri, K. (2012). NIH Image to ImageJ: 25 years of image analysis. Nat. Methods *9*, 671–675. https://doi.org/10.1038/nmeth.2089.

Schoof, E.M., Furtwängler, B., Üresin, N., Rapin, N., Savickas, S., Gentil, C., Lechman, E., Keller, U.a. d., Dick, J.E., and Porse, B.T. (2021). Quantitative single-cell proteomics as a tool to characterize cellular hierarchies. Nat. Commun. *12*, 3341. https://doi.org/10.1038/s41467-021-23667-y.

Sollazzo, A., Brzozowska, B., Cheng, L., Lundholm, L., Scherthan, H., and Wojcik, A. (2018). Live dynamics of 53BP1 foci following simultaneous induction of clustered and dispersed DNA damage in U2OS cells. Int. J. Mol. Sci. *19*, 519. https://doi.org/10.3390/ijms19020519.

Specht, H., Harmange, G., Perlman, D.H., Emmott, E., Niziolek, Z., Budnik, B., and Slavov, N. (2018). Automated sample preparation for high-throughput single-cell proteomics. Preprint at bioRxiv. https://doi.org/10.1101/399774.

Tirosh, I., Izar, B., Prakadan, S.M., Wadsworth, M.H., 2nd, Treacy, D., Trombetta, J.J., Rotem, A., Rodman, C., Lian, C., Murphy, G., et al. (2016). Dissecting the multicellular ecosystem of metastatic melanoma by single-cell RNA-seq. Science *352*, 189–196. https://doi.org/10.1126/science.aad0501.

Tsai, C.F., Zhao, R., Williams, S.M., Moore, R.J., Schultz, K., Chrisler, W.B., Pasa-Tolic, L., Rodland, K.D., Smith, R.D., Shi, T., et al. (2020). An improved boosting to amplify signal with isobaric labeling (iBASIL) strategy for precise quantitative single-cell proteomics. Mol. Cell. Proteomics *19*, 828–838. https://doi.org/10.1074/mcp.ra119.001857.

Tyanova, S., Temu, T., Sinitcyn, P., Carlson, A., Hein, M., Geiger, T., Mann, M., and Cox, J. (2016). The Perseus computational platform for comprehensive analysis of (prote)omics data. Nat. Methods *13*, 731–740. https://doi.org/10.1038/nmeth.3901.

Vistain, L.F., and Tay, S. (2021). Single-cell proteomics. Trends Biochem. Sci. *46*, 661–672. https://doi.org/10.1016/j.tibs.2021.01.013.

You, L., Su, P.-R., Betjes, M., Rad, R.G., Chou, T.-C., Beerens, C., van Oosten, E., Leufkens, F., Gasecka, P., Muraro, M., et al. (2022). Linking the genotypes and phenotypes of cancer cells in heterogenous populations via real-time optical tagging and image analysis. Nature Biomed. Eng. https://doi.org/10.1038/s41551-022-00853-x.

Zhu, Y., Piehowski, P.D., Zhao, R., Chen, J., Shen, Y., Moore, R.J., Shukla, A.K., Petyuk, V.A., Campbell-Thompson, M., Mathews, C.E., et al. (2018). Nanodroplet processing platform for deep and quantitative proteome profiling of 10-100 mammalian cells. Nat. Commun. *9*, 882. https://doi.org/10.1038/s41467-018-03367-w.

STAR★METHODS

KEY RESOURCES TABLE

REAGENT or RESOURCE	SOURCE	IDENTIFIER
Antibodies		
Rabbit polyclonal anti-PDS5A	Novus	Cat#NBP1-87904; RRID: AB_11015600
Rabbit polyclonal anti-γH2AX	Abcam	Cat#ab11174; RRID: AB_297813
Goat polyclonal Alexa-488 anti-rabbit	Abcam	Cat#ab150077; RRID: AB_2630356
Chemicals, peptides, and recombinant proteins		
DMEM medium	Thermo Fisher	Cat#11965092
Lipofectamine 3000 Transfection Reagent	Thermo Fisher	Cat#L3000001
Fetal bovine serum	Thermo Fisher	Cat#A4736301
Penicillin-Streptomycin	Thermo Fisher	Cat#15140122
FluoroBrite DMEM medium	Thermo Fisher	Cat#A1896701
PA Janelia Fluor 646, SE	Tocris Bioscience	Cat#6150
Triethylammonium bicarbonate buffer	Sigma-Aldrich	Cat#T7408
Water, LC-MS Grade	Thermo Fisher	Cat#51140
Acetonitrile (ACN), LC-MS Grade	Thermo Fisher	Cat#51101
TMT10plex Isobaric Label Reagent Set	Thermo Fisher	Cat#90110
Hydroxylamine solution	Sigma-Aldrich	Cat#467804
Formic acid	Sigma-Aldrich	Cat#33015-M
Deposited data		
Raw and analyzed data	This paper	ProteomeXchange: PXD034370
Experimental models: Cell lines		
Human: U2OS cells transfected with PB-mScarlet-53BP1	Erasmus University Medical Center, Molecular Genetics	N/A
Software and algorithms		
Automatic cell tracking analysis	You et al. (2022)	https://sourceforge.net/projects/funseq/
ImageJ	Schneider et al. (2012)	https://imagej.nih.gov/ij/
Matlab	MathWorks	https://nl.mathworks.com/products/matlab.html
MaxQuant	Cox and Mann (2008)	https://www.maxquant.org/
Perseus	Tyanova et al. (2016)	https://www.maxquant.org/perseus/
Other		
Orbitrap Eclipse Tribid mass spectrometer	Thermo Fisher	http://thermofisher.com/OrbitrapEclipse

RESOURCE AVAILABILITY

Lead contact

Further information and requests for resources and reagents should be directed to and will be fulfilled by the lead contact: Miao-Ping Chien (m.p.chien@erasmusmc.nl).

Materials availability

53BP1-mScarlet plasmid generated in this study is available via the lead contact upon request.

Data and code availability

- The mass spectrometry proteomics raw data as well as protein and peptide ID lists have been deposited in the ProteomeXchange Consortium database (http://proteomecentral.proteomexchange.org) with the dataset identifier PXD034370.
- No new code was generated in this paper.
- Any additional information required to reanalyze the data reported in this paper is available from the lead contact upon request.

CellPress
OPEN ACCESS

EXPERIMENTAL MODEL AND SUBJECT DETAILS

U2OS cells

Human bone osteosarcoma cell line U2OS was stably transfected with PB-mScarlet-53BP1 (a gift from Hanny Odijk) using Lipofectamine 3000 (Thermo Fisher), under puromycin selection (1 μg/mL). The stable cells were cultured in DMEM supplemented with 10% fetal bovine serum and 1% penicillin/streptomycin in a 37°C incubator under 5% CO_2.

METHOD DETAILS

Ultrawide field-of-view optical microscope

The ultrawide field-of-view optical (UFO) microscope is a custom-built microscope and has been described in detail previously (You et al., 2022). Here, we upgraded the system to have a higher spatial resolution by implementing an objective with a large field-of-view (FOV) and relatively high numerical aperture (Olympus MVP Plan Apochromat 1×, 0.5 NA) in conjunction with a large chip-size cMOS camera with small pixel-size (Grasshopper3, FLIR, 4096 × 3000 pixels, 3.25 μm/pixel). UFO provides a 3.65 × 2.83 mm FOV with 0.8 μm/pixel spatial resolution and 30 ms/frame temporal resolution.

Illumination source was provided by CW laser lines including 405 nm (MDL-HD-405/2W, CNI), 532 nm (MGL-FN-532/1500 mW, CNI) and 637 nm (MDL-MD-637/1.3W, CNI). The lasers were modulated, in wavelength-selection, temporality and intensity, by an acousto-optic tunable filter (Gooch & Housego). Fluorescence was filtered through a custom-designed 2″ tri-band emission filter (Od6avg: 400-465/527-537/632-642/785-1300 nm, Alluxa), where filter switching is not needed.

Cell preparation, radiation and live imaging on the UFO microscope

Prior to imaging, U2OS 53BP1-mScarlet cells were seeded in FluoroBrite DMEM supplemented with 10% fetal bovine serum and 1% penicillin/streptomycin at 500k in a 35 mm plastic dish with a 10 mm glass bottom (Cellvis) 1 day in advance. The glass-bottom dish was pre-coated with 0.2% gelatin. The cells were cultured in a 37°C incubator under 5% CO_2. The mini-incubator at the UFO microscope was equilibrated at 37°C and 5% CO_2 prior to imaging. For subsequent phototagging, the cells were pre-incubated with 30 μM photoactivable Janelia Fluor 646 (Bio-Techne) for 15 min, which can be photoactivated by 405 nm laser and visualized by 637 nm laser (λ_{ex}: 650 nm; λ_{em}: 664 nm). The stained cells were rinsed and incubated in the original medium. Time-lapse movie was recorded by 532 nm laser with interval time of 3 min for 1 h before ionizing radiation. After that, the cells were irradiated with a radiation dose of 2 Gy at a dose-rate of 1.67 Gy/min (RS320, Xstrahl Medical & Life Sciences). The cells were put back in the mini-incubator at UFO immediately after radiation and registered back to the previous position. The cells were then recorded by 532 nm laser illumination with interval time of 3 min for 24 h.

Target cell photolabeling and isolation

The image analysis was completed within 10 min after the last image frame of a time-lapse movie. The coordinates (in pixels) of cells of interest identified from the image analysis were then uploaded to the program, which then controlled a pair of galvo mirrors (Cambridge Technology) and steered the selective illumination pattern of 405 nm laser (3 J/cm^2) onto the cells of interest. Upon 2 s selective illumination, the phototagging reagent inside the cells under illumination was photoactivated (the whole phototagging process took less than a minute). The photoactivated cells were invariably visualized by 637 nm laser (λ_{ex}: 650 nm; λ_{em}: 664 nm), while other cells remained dark. After this, all the cells in the whole dish were immediately dissociated with trypsin followed by fluorescence-activated cell sorting (BD Biosciences), whereby photoactivated cells were isolated together with a similar amount of non-photoactivated control cells.

Single-cell proteomics

SCoPE-MS (Budnik et al., 2018) has been widely adapted and optimized in sample preparation, liquid chromatography and MS settings (Zhu et al., 2018; Cong et al., 2020; Tsai et al., 2020). SCoPE-MS combines the tandem mass tag (TMT) technology with an addition of carrier cells to identify and quantify peptides/proteins of single cells. We prepared the sample using the minimal ProteOmic sample Preparation method (mPOP (Specht et al., 2018)): a 96-well plate pre-filled with 20 μL pure water and sorted with designated cells per well was frozen on dry ice for 5 min and heated by ThermoMixer C (Eppendorf) at 95°C for 10 min followed by spinning down at 3000 rpm for 1 min. 20 μL of 100 mM triethylammonium bicarbonate buffer (TEABC, Sigma-Aldrich) was added to each well of the plate, and 1 and 2 μL of 50 ng/μL trypsin (in 100 mM TEABC, Promega) was added to the wells with single cells and two hundred carrier cells, respectively. Digestion was performed at 37°C ThermoMixer C with shaking speed at 650 rpm overnight. After digestion, the 96-well plate was then spun down at 3000 rpm for 1 min.

0.5 and 1 μL of 85 mM TMT labeling reagent (TMT10plex, Thermo Fischer) was then added to the wells with single cells and two hundred carrier cells, respectively. The labeling was performed at 25°C with shaking speed of 650 rpm for 1 h. After labeling, 0.5 μL of 5% (v/v) hydroxylamine was added to each well, and the TMT labeling reaction was quenched at 25°C with shaking speed at 650 rpm for 15 min. All corresponding samples were combined into the same wells, respectively. 1 μL of 10% (v/v) formic acid (FA, Sigma-Aldrich) was added to each combined well. After acidifying, the samples were desalted by μ-C18 ZipTip (EMD Millipore) and kept in the ZipTip at −80°C before the MS analysis.

Prior to the MS analysis, the samples were eluted by 50% (v/v) acetonitrile (ACN, Sigma-Aldrich) and speed-vacuum dried. The samples were resuspended with 0.1% (v/v) FA. Nanoflow liquid chromatography tandem mass spectrometry (LC-MS/MS) was performed on an EASY-nLC 1200 (Thermo Fischer) coupled to an Orbitrap Eclipse Tribrid mass spectrometer (Thermo Fischer) operating in positive mode. Peptide mixtures were trapped on a 2 cm × 100 μm PepMap C18 column (Thermo Fisher 164564) and then separated on an in-house packed 50 cm × 75 μm capillary column with 1.9 μm ReproSil-Pur C18 beads (Dr. Maisch) at a flowrate of 250 nL/min, using a linear gradient of 0–32% acetonitrile (in 0.1% formic acid) during 120 min. The MS was performed in the data-dependent acquisition mode. Surveying full scan (MS1) was in the range of 375–1,400 *m/z* and the resolution was set to 120k. Fragmentation of the peptides was performed by HCD. The resolution of tandem mass spectrum (MS2) was set to 30k, automatic gain control (AGC) was 5E4 and the maximum injection time (IT) was 300 ms (Figure S2A).

The mass spectrometry proteomics raw data as well as protein and peptide ID lists have been deposited in the ProteomeXchange Consortium database (http://proteomecentral.proteomexchange.org) with the dataset identifier PXD034370.

Immunofluorescence staining and analysis

Cells were prepared as the abovementioned cell preparation method. After IR the cells were immediately imaged for 24 h followed by cell fixation with 4% formaldehyde (v/v) in PBS. After fixation the cells were rinsed with PBS containing 0.1% (v/v) Triton followed by incubating with 0.15% (w/w) glycine and 0.5% (w/w) BSA to block non-specific binding sites of the cells. The cells were then incubated with 1:500 rabbit polyclonal anti-PDS5A antibody (Novus) or 1:1000 rabbit polyclonal anti-γH2AX antibody (Abcam) for 90 min at room temperature. After antibody incubation the cells were washed with PBS containing 0.1% (v/v) Triton and then incubated with 1:1000 goat polyclonal Alexa-488 anti-rabbit antibody (Abcam) for 60 min at room temperature under dark environment; after that, the cells were then rinsed with PBS containing 0.1% Triton and stored in PBS before imaging. The fixed cells were imaged by a confocal microscope (SP5, Leica); Alexa 488 and mScarlet were excited by the 488 and 561 nm lasers, respectively, and imaged by a photomultiplier tube (PMT) with emission spectra setting at 500–550 nm and 570–600 nm, respectively. The protein expression level of individual cells was quantified by the summation intensity projection of fluorescence intensity. Group 2 cells were computed against the same amount of randomly selected Group 1 cells and the significance was computed using the two-tailed t-test.

QUANTIFICATION AND STATISTICAL ANALYSIS

Automatic foci detection analysis

The foci detection algorithm is a modified local comparison method (Ruusuvuori et al., 2010) (Figure S1, Table S1). It first generated a reference image from maximum intensity projection of four convoluted images (the raw image was filtered with four different Gaussian-like filter kernels; Figures S1A and S1B), and then created a normalized reference image by dividing the reference image with a sensitivity factor α. The sensitivity factor α (0.31) and the radius of filter size (3 pixels) were determined based on the highest F score by sweeping the value of sensitivity factor α from 0 to 1 and the filter size from 0 to 20 pixels, respectively (Figure S1C). The foci logical (binary) image was then calculated by Boolean expression (true: when the normalized reference image is greater than the original image; Figure S1A). The detected foci located within a nuclear boundary were registered to the designated nuclei. The number of foci were calculated and plotted over time. Euclidean distance-based hierarchical clustering was used to classify clusters with different trends of foci dynamics. The integrated foci and cell tracking analysis output the coordinates (in pixels) of target cells with desired features, including cells with rising DDR foci. Cells displaying up & down DDR foci dynamics trend were classified as Group 1; cells with rising DDR foci trend were classified as Group 2.

Automatic cell tracking analysis

To reduce interference from foci when tracking individual cell nuclei, we applied the foci detection algorithm to identify the locations (pixels) of individual foci within each cell nucleus from raw images and removed and replaced them with their neighboring pixels before smoothing the inhomogeneous background within nuclei. We then pre-processed the image using top-hat filtering, local comparison and selection, local brightness adjustment and edge-preserving smoothing to improve accuracy and sensitivity of cell segmentation and tracking. After the foci-dedicated pre-processing, we then applied the mTGMM algorithm for cell segmentation and tracking: we first applied watershed thresholding to find nuclei foreground pixels. The connected foreground pixels were grouped as a single superpixel. All superpixels were trimmed by local Otsu's thresholding. If more than two superpixels were still connected after thresholding, then they would be grouped together as one. Each final superpixels were fit into Gaussian mixture models (GMMs) separately. With this approach, individual cell nuclei were modeled as GMMs and can be accurately segmented with high precision and recall rate (Precision: 98.1%, Recall: 97.7%, F score: 97.9%, IoU: 95.8%).

The cell tracking was done by forwarding every GMM from time point t to $t + 1$ using Bayesian inference, which is, comparing central position, shape, and overall intensity. After cells were tracked, information of cellular characteristics and dynamics including nuclear properties (central position, area, orientation, circularity and intensity), cell division and cell lineage were exported to a feature table. Dividing or apoptotic cells were filtered out during the analysis to perform the Euclidean distance-based hierarchical clustering.

We then applied the integrated foci detection and mTGMM tracking algorithms to simultaneously track cellular movement (with tracking accuracy: 97.7%) while monitoring DDR foci dynamics within each cell nucleus and maintain the processing speed of ~57,000 cells/min. Dividing or dead cells were filtered out during the analysis before performing the Euclidean distance-based

hierarchical clustering. All images were processed by MATLAB and C++. The image analyses were performed in real-time while acquiring live-cell imaging.

Proteomics analysis

Raw MS data were processed with MaxQuant (version 2.0.3.1): peptides were searched against SwissProt database (*Homo sapiens*, downloaded on 2021/10/8), static modification was left empty, variable modifications were deamidation (NQ) and oxidation (M), and minimum peptide length was 7. The reporter ion MS2 analysis was used with the isotopic impurity correction factors provided by the manufacturer (TMT batch number: VB287465). The peptide-spectrum match (PSM)-level weighted ratio normalization and match between runs were used for identification. Other parameters were remained default. The proteins were filtered at 1% protein identification false discovery rate (FDR). Subsequently, the protein groups, peptide list, and PSMs were exported from MaxQuant for further processing. The protein groups list was further imported into Perseus (version 1.6.14.0) for differential protein analysis. The reversed proteins and contaminant proteins were removed, the proteins identified in less than 3 cells were removed, after which 2,129 unique proteins (10,575 unique peptides) were identified. After filtering, the cell types (Group 1 or Group 2) were annotated, the intensity was log2-transformed and normalized by subtracting the medians of columns and rows sequentially. The differential protein analysis by two-tailed t-test was computed, and significantly up-regulated proteins (FDR $\leq$0.05) were reported and highlighted in the volcano plot (Figure 4C).

Quality and quantitative accuracy of the single-cell proteomics data

The reporter ion density in the single-cell channels was checked to be statistically higher (t-test, $p \leq 0.001$) than in the blank channels (PBS only) (Figure S2B). No effect on quantitative accuracy was observed for the composition of carrier cells (a mix of non-IR and IR cells, non-IR only cells and IR only cells) as the median of mean signal-to-noise (S/N) and coefficient of variations (CV) values (according to the method described in Schoof et al. (2021)) were similar in these three samples with different compositions of carrier cells (Figure S3A). Furthermore, the quality of the data was similar to the data shown in Schoof et al. (2021) (the 300 ms-injection time setting used in this work). In addition, no clear effect of phototagging was observed as the S/N and CV values were similar between the phototagging and non-phototagging groups from the single-cell data (Figure S2C) and a high correlation was observed between the phototagging and non-phototagging group from the bulk cell data (Pearson correlation r = 0.977) (Figure S2D).

Statistical analysis

Exact value of N for each data can be found in individual figure captions. Line plots were used for visualization of DDR dynamics trends with indicated mean (bold lines) and standard deviation (shaded area). Volcano plots were used for visualization of differentially expressed gene with indicated cutoff of permutation-based FDR at 0.05 (dashed lines). Box plots were used for visualization of data distribution with indicated 25th and 75th percentiles of the data (lower and upper edges of the box), median (central line), data points (filled circles) and outliers (open circles). Statistical significances were determined by performing two-tailed Student's *t* test. Asterisks represent following p-values: ns - $p > 0.05$; * - $p \leq 0.05$; ** - $p \leq 0.01$; *** - $p \leq 0.001$.